AGU PUBLICATIONS

Water Resources Research

RESEARCH ARTICLE
10.1002/2013WR014057

Key Points:
- Chaotic advection produces plume spreading in aquifers
- Heterogeneity increases spreading in a chaotic flow
- Plume geometry aligns with unstable manifolds of periodic points in chaotic flow

Correspondence to:
R. M. Neupauer,
neupauer@colorado.edu

Citation:
Neupauer, R. M., J. D. Meiss, and D. C. Mays (2014), Chaotic advection and reaction during engineered injection and extraction in heterogeneous porous media, *Water Resour. Res.*, *50*, doi:10.1002/2013WR014057.

Received 1 MAY 2013
Accepted 4 FEB 2014
Accepted article online 8 FEB 2014

Chaotic advection and reaction during engineered injection and extraction in heterogeneous porous media

Roseanna M. Neupauer[1], James D. Meiss[2], and David C. Mays[3]

[1]Department of Civil, Environmental, and Architectural Engineering, University of Colorado Boulder, Boulder, Colorado, USA, [2]Department of Applied Mathematics, University of Colorado Boulder, Boulder, Colorado, USA, [3]Department of Civil Engineering, University of Colorado Denver, Denver, Colorado, USA

Abstract During in situ remediation of contaminated groundwater, a treatment solution is often injected into the contaminated region to initiate reactions that degrade the contaminant. Degradation reactions only occur where the treatment solution and the contaminated groundwater are close enough that mixing will bring them together. Degradation is enhanced when the treatment solution is spread into the contaminated region, thereby increasing the spatial extent of mixing and degradation reactions. Spreading results from local velocity variations that emerge from aquifer heterogeneity and from spatial variations in the external forcings that drive flow. Certain patterns in external forcings have been shown to create chaotic advection, which is known to enhance spreading of solutes in groundwater flow and other laminar flows. This work uses numerical simulations of flow and reactive transport to investigate how aquifer heterogeneity changes the qualitative and quantitative aspects of chaotic advection in an aquifer, and the extent to which these changes enhance contaminant degradation. We generate chaotic advection using engineered injection and extraction (EIE), an approach that uses sequential injection and extraction of water in wells surrounding the contaminated region to create time-dependent flow fields that promote plume spreading. We demonstrate that as the degree of heterogeneity increases, both plume spreading and contaminant degradation increase; however, the increase in contaminant degradation is small relative to the increase in plume spreading. Our results show that the combined effects of EIE and heterogeneity produce substantially more stretching than either effect separately.

1. Introduction

During in situ remediation of contaminated groundwater, a treatment solution is often injected into the contaminated region to initiate reactions that degrade the contaminant. Degradation reactions only occur where the treatment solution and the contaminated groundwater are close enough that mixing will bring them into contact with each other. Spreading the treatment solution throughout the contaminated region increases the extent to which the treatment solution and contaminated groundwater are close enough that mixing will bring them into contact. In this context, we use the term spreading to describe the changes in the plume shape as a result of spatially varying velocity [e.g., *Le Borgne et al.*, 2010]. Spreading leads to an irregularly shaped treatment solution plume that is interfingered with the contaminant plume; however, it does not change the volume of the plume. We use the term mixing to refer to the molecular diffusion and transverse dispersion processes that bring the treatment solution and contaminated groundwater together, increasing the volume occupied by each of the plumes. Spreading does not promote reaction directly; rather it creates concentration fronts between the treatment solution and the contaminated groundwater that can be smoothed out by mixing [e.g., *Cirpka et al.*, 2011; *Dentz et al.*, 2011]. The combination of spreading and mixing controls the overall rate of the degradation reactions [e.g., *De Simoni et al.*, 2005; *Cirpka et al.*, 2008; *Luo et al.*, 2008].

Groundwater velocity is described by Darcy's law which, for a two-dimensional, confined aquifer with essentially horizontal flow (i.e., the conceptual model we consider in this work), is given by

$$\mathbf{v} = -\frac{T}{nb}\nabla h, \tag{1}$$

where $\mathbf{v}$ is the groundwater velocity vector, n is porosity, b is the aquifer thickness, T is the aquifer transmissivity (here assumed to be isotropic but not necessarily homogeneous), and ∇h is the gradient of the hydraulic head, h. The head gradient is obtained by solving the groundwater flow equation, given by

$$S\frac{\partial h}{\partial t} = \nabla \cdot T\nabla h + F, \quad (2)$$

where S is the storage coefficient, t is time, and F represents all sources and sinks of water.

From (1), the spatial variations in velocity that lead to spreading in porous media can be caused by heterogeneity of material properties such as transmissivity [e.g., *Gelhar and Axness*, 1983; *Dagan*, 1984, 1989] or by spatial variations in the hydraulic gradient that result from spatial variations in the sources and sinks or boundary conditions on (2). Thus, even in a homogeneous aquifer, velocity variations that lead to spreading can occur.

Chaotic advection forms a special class of flows that create velocity variations that lead to spreading in laminar flows, including groundwater flow [*Ottino et al*., 1994]. Within chaotic regions of a flow, fluid particles exhibit sensitive dependence on initial conditions; in other words, fluid particles that are initially adjacent to each other can follow radically different flow paths, leading to spreading of initially nearby fluid particles.

Some of the dynamically important invariant sets of a chaotic flow include its periodic points and their invariant manifolds. A fluid particle lies on an orbit of period N when it returns to its initial location after N cycles of the periodic flow. Such an initial condition is a periodic point of period N, or simply a period N point [*Tabor*, 1989]. In two-dimensional incompressible flow, periodic points are classified as either elliptic or hyperbolic. Elliptic periodic points characterize regions of poor spreading. A fluid parcel in the neighborhood of an elliptic periodic point returns back to the neighborhood of the periodic point with negligible deformation. Hyperbolic periodic points, on the other hand, characterize regions of good spreading. A fluid parcel in the neighborhood of a hyperbolic periodic point exhibits substantial deformation, being stretched in one direction and compressed in another direction, while preserving its volume.

The deformation of a fluid parcel in the neighborhood of a hyperbolic periodic point is closely tied to its stable and unstable manifolds. A stable manifold is the collection of points that approach the hyperbolic periodic point upon many subsequent iterations of the periodic flow; while an unstable manifold is the collection of points that converge to the periodic point in backward time [e.g., *Tabor*, 1989]. Thus, when a fluid parcel returns to the neighborhood of a hyperbolic periodic point, it is stretched along the direction of the unstable manifold and is compressed along the direction of the stable manifold.

In a two-dimensional domain, chaotic advection can only be created with time-dependent flows. The simplest models for chaotic flows are periodically time dependent, and chaos is defined in terms of an infinite-time limit. Since such an infinite-time limit is not physically meaningful for groundwater remediation problems, a more appropriate model for our applications is a transitory flow [*Mosovsky and Meiss*, 2011], in which the flow is time-dependent only for a finite period. This period might correspond to the duration of an active groundwater remediation process. The characteristics of chaos (e.g., sensitivity to small deviations) can still be present during the transitory regime; however, they vanish after the system returns to a steady state. In this context, the term "periodic point" can be replaced with "recurrent point," identifying points where fluid returns to its original position after the transition interval.

Some methods for creating chaotic flow that have been investigated in groundwater modeling studies include a pulsed dipole [*Jones and Aref*, 1988; *Tel et al*., 2000; *Stremler et al*., 2004; *Sposito*, 2006], a rotating pulsed dipole [*Trefry et al*., 2012], oscillatory flow in a well triplet [*Bagtzoglou and Oates*, 2007], and engineered injection and extraction [*Mays and Neupauer*, 2012]. In all of these works, the aquifer was assumed to be homogeneous.

Since all aquifers exhibit some degree of heterogeneity, the goal of this paper is to investigate the degree to which heterogeneity enhances spreading in a chaotic groundwater flow. We limit our analysis to two-dimensional systems because chaotic advection in three-dimensional systems has not been well studied [e.g., *Wiggins*, 2010]. To create time-dependent flow, we use engineered injection and extraction (EIE), in which a treatment solution that degrades the contaminant is emplaced within the contaminated region of the aquifer, and wells installed around the contaminated region are operated sequentially to either inject clean water or to extract groundwater. *Mays and Neupauer* [2012] showed that during EIE in a homogeneous aquifer, the interface between the treatment solution and contaminated groundwater aligns with the unstable manifolds of periodic points as treatment solution is spread into the contaminated region. This spreading leads to a fivefold to sixfold increase in the amount of contaminant degradation relative to the

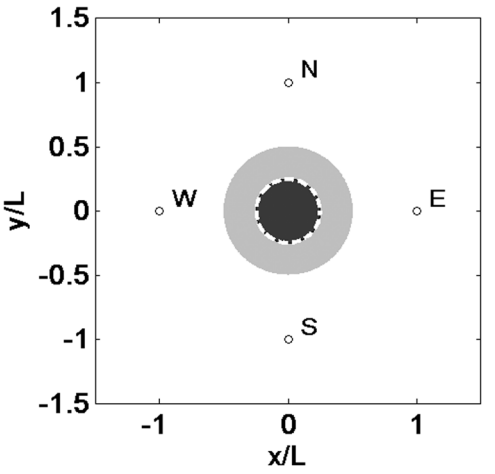

Figure 1. Plan view of the engineered injection and extraction system. Small circles represent well locations; the labels identify the wells. The light gray region is the initial contaminant plume; the dark gray region is the initial position of the treatment solution plume; and the dashed white circle represents the initial interface between the treatment solution and the contaminated aquifer.

amount occurring with in situ remediation practices without EIE [*Piscopo et al*., 2013]. In heterogeneous aquifers, *Piscopo et al*. [2013] found that the amount of contaminant degradation during EIE is larger than the amount that occurs during EIE in a homogeneous aquifer, presumably due to additional spreading caused by heterogeneity. However, they did not study how aquifer heterogeneity impacts the characteristics of chaotic advection itself.

In this paper, we analyze the characteristics of chaotic advection, including the period one points (or, equivalently, the recurrent points) and their associated manifolds for one cycle of an EIE sequence in one homogeneous aquifer and nine different models of heterogeneous aquifers. We demonstrate that heterogeneity increases the spatial extent and local efficiency of spreading. In particular, we demonstrate that as the degree of heterogeneity increases, the stretching in the vicinity of the periodic points increases.

In natural systems, chemicals experience both advective and dispersive transport. To investigate the combined effects of advection, dispersion, and reaction, we also simulate the advective-dispersive-reactive transport of treatment solution and contaminant during EIE, and we show that the amount of contaminant degradation increases as heterogeneity increases. Note, however, that when we analyze the features of chaotic advection, we ignore dispersion because it does not play a role in chaotic advection.

In the next section, we discuss the EIE system, the numerical methods used to simulate flow and transport during EIE, and the heterogeneous aquifer models used in this study. Next, we evaluate several measures of stretching, quantify the amount of degradation reactions for each heterogeneous aquifer model, and demonstrate the relationship between heterogeneity and these measures. Finally, we discuss the implications of these results on the remediation of contaminated aquifers using EIE.

2. Approach

2.1. Engineered Injection and Extraction

We evaluate engineered injection and extraction for a two-dimensional, horizontal confined aquifer. We use four wells, as shown in Figure 1, which surround a contaminated region of the aquifer. Treatment solution is emplaced in the center of the contaminated region with the initial geometry shown in Figure 1. The treatment solution is distributed uniformly with a concentration of 25.3 mg/m^3 within the circular region of radius 6.25 m centered at the origin, and the contaminant is distributed uniformly at a concentration of 6.4 mg/m^3 in an annular region with outer radius of 12.5 m and inner radius of 6.25 m. In Figure 1 and other figures, the axes are in dimensionless distances, x/L and y/L, where L is the distance between any well and the origin. In this work, we use $L = 25$ m. A similar initial configuration was also used by *Mays and Neupauer* [2012] and *Piscopo et al*. [2013].

We use the EIE sequence shown in Table 1, which was also used by *Mays and Neupauer* [2012] and *Piscopo et al*. [2013]. This sequence was developed heuristically to generate good spreading by both stretching the fluid interface and folding the fluid interface (see Figure 2). In the first six steps of the sequence, the east and west wells are operated to create a fold along the x axis. In the last six steps, the process is repeated with the north and south wells to create another fold along the y axis. Although other well configurations and injection and extraction sequences can also be used in EIE, we focus on this sequence because it has been shown to create folding, and it serves as a base case from which we can investigate the degree to which heterogeneity affects spreading.

Table 1. Engineered Injection and Extraction Sequence

Step	Active Well	Injection Rate (m^3/d)
1	W	875
2	E	875
3	W	−250
4	E	−750
5	W	−400
6	E	−350
7	S	875
8	N	875
9	S	−250
10	N	−750
11	S	−400
12	N	−350

2.2. Flow and Transport Modeling

The model domain is square with constant head boundaries of equal value on the east and west sides and no-flow boundaries on the north and south sides; thus, there is no ambient flow in this system. The domain is sufficiently large that the boundary conditions do not affect the simulation results; indeed, the final interface geometry from the numerical simulation for a homogeneous system is visually indistinguishable from the final interface geometry obtained from the analytical model of *Mays and Neupauer* [2012]. Parameter values and domain geometry used in the simulations are shown in Table 2.

Transport of the contaminant and treatment solution is governed by the advection-dispersion-reaction equation, given by:

$$\frac{\partial C_j}{\partial t} = -\nabla \cdot (\mathbf{v} C_j) + \nabla \cdot \mathbf{D} \nabla C_j - R, \tag{3}$$

where C_j is the concentration of component j ($j = 1$ represents the treatment solution and $j = 2$ represents the contaminant), $\mathbf{v} = (v_x, v_y)$ is the velocity vector which comes from (1) and (2), R is the reaction rate, and $\mathbf{D}$ is the dispersion tensor, given by:

$$D_{xx} = \alpha_L \frac{v_x^2}{|\mathbf{v}|} + \alpha_T \frac{v_y^2}{|\mathbf{v}|}, \tag{4}$$

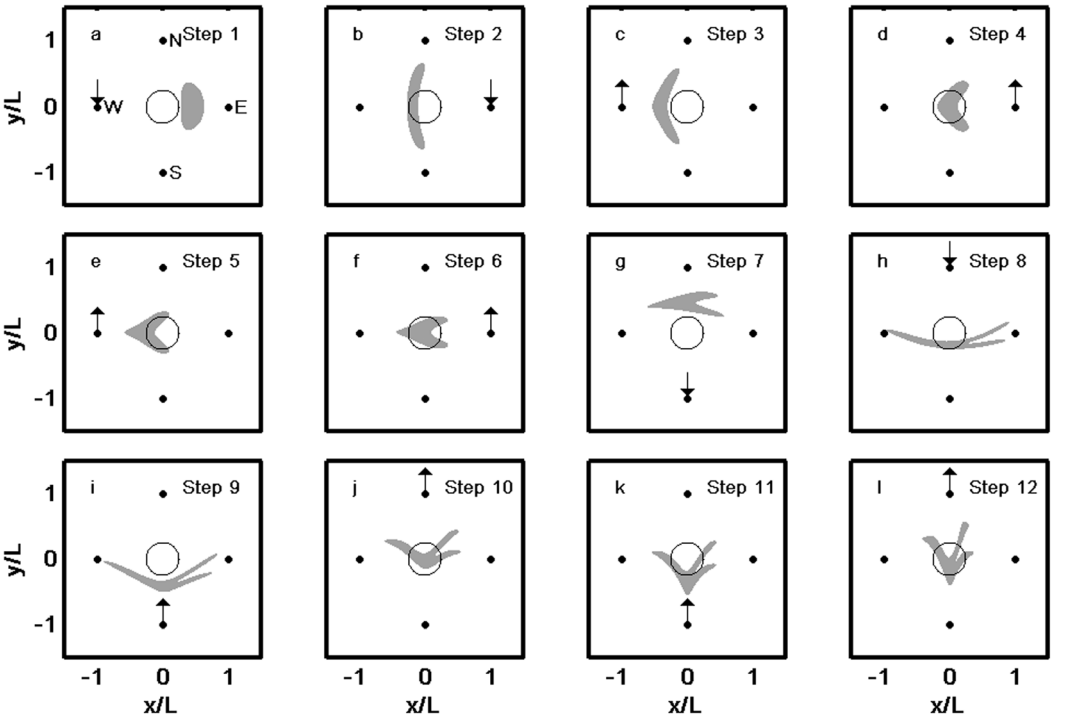

Figure 2. Position of the treatment solution plume (gray) after each step of the EIE sequence in the homogeneous aquifer. The open black circles show the initial position of the treatment solution plume. Small filled black circles show the well locations. The arrow denotes the active well, with injection indicated by a downward pointing arrow and extraction indicated by an upward pointing arrow (adapted from *Mays and Neupauer* [2012]).

Table 2. Parameter Values Used in the Simulations

Parameter	Value
Distance from origin to well, L	25 m
Storage coefficient, S	1×10^{-5}
Mean transmissivity, T	0.5 m^2/d
Aquifer top elevation	0 m
Aquifer bottom elevation	−10 m
Aquifer thickness, b	10 m
Porosity, n	0.25
Duration of EIE step	6.25 day
Dimensions of the model domain	$-150.125\ \text{m} \le x \le 150.125\ \text{m}$
	$-150.125\ \text{m} \le y \le 150.125\ \text{m}$
Finite difference grid spacing	0.25 m × 0.25 m
Flow boundary conditions	h = 10 m on east and west
Ambient velocity	0
Longitudinal dispersivity, α_L	0.05 m
Transverse dispersivity, α_T	0.005 m
Initial concentration of treatment solution	25.3 mg/m^3
Initial concentration of contaminant	6.4 mg/m^3

$$D_{xy} = D_{yx} = (\alpha_L - \alpha_T)\frac{v_x v_y}{|\mathbf{v}|}, \quad (5)$$

$$D_{yy} = \alpha_L \frac{v_y^2}{|\mathbf{v}|} + \alpha_T \frac{v_x^2}{|\mathbf{v}|}, \quad (6)$$

where α_L and α_T are the longitudinal and transverse dispersivities, respectively. We solve (3) using a random walk approach. We use MODFLOW-2000 [*Harbaugh et al*., 2000] to solve the groundwater flow equation (2) with the source and sink term given by:

$$F = Q_i \delta(x - x_{wi})\delta(y - y_{wi}), \quad (7)$$

where Q_i is the injection rate at step i of the EIE sequence ($Q_i < 0$ implies extraction), (x_{wi}, y_{wi}) is the location of the active well at step i, and $\delta(\cdot)$ is the Dirac delta function. The resulting velocity field from (1) is used in MODPATH [*Pollock*, 1994] to track the advective movement of fluid particles in that flow field. Simulation of the dispersion and reaction processes follows the same approach as *Piscopo et al*. [2013]. We assume an instantaneous, irreversible bimolecular reaction given by:

$$C_1 + C_2 \rightarrow C_3. \quad (8)$$

2.3. Aquifer Models

For the heterogeneous aquifers in this work, we consider nine different models of random ln T fields generated using sequential Gaussian simulation with GSLIB [*Deutsch and Journel*, 1992] with a spherical variogram with variances of ln T of $\sigma^2_{\ln T} = 0.1$, 0.2, and 0.3, and correlation lengths of $\lambda = 3.125$, 6.25, and 12.5 m. For the nine different heterogeneity models, we use each combination of variance and correlation length. We generate 30 realizations of each heterogeneity model, using the same set of random number seeds. All aquifer models, including the homogeneous aquifer, have a mean T of 0.5 m^2/d. A single realization of each heterogeneity model is shown in Figure 3.

3. Results

We analyzed the performance of the EIE sequence shown in Table 1 in the homogeneous aquifer and the nine heterogeneous aquifers. The results presented in this section discuss the resulting fluid interfaces, periodic orbits, amount of contaminant degradation, and the relationships among these features.

3.1. Fluid Interface

Since degradation reactions occur only within a narrow band along the interface between the treatment solution and contaminated groundwater, a goal of EIE is to elongate this fluid interface. We simulated the movement of the fluid interface by representing the initial interface (shown in Figure 1) with 10,000 uniformly spaced numerical particles, and tracked the advective movement of these particles through the EIE sequence. During the tracking, if the separation distance between any two adjacent particles exceeded 10 times the initial separation distance, new particles were inserted following the approach of *Schafer-Perini and Wilson* [1991].

The position and geometry of the fluid interface is shown in Figure 2 for the homogeneous aquifer. Since this EIE sequence produces two folds, the final geometry of the fluid interface in the homogeneous aquifer is a three-branched shape. During injection, the interface generally moves radially away from the active well; while during extraction, it generally moves radially toward the active well. In heterogeneous aquifers, the heterogeneity causes local variations in the plume movement that result in deviations from radial flow.

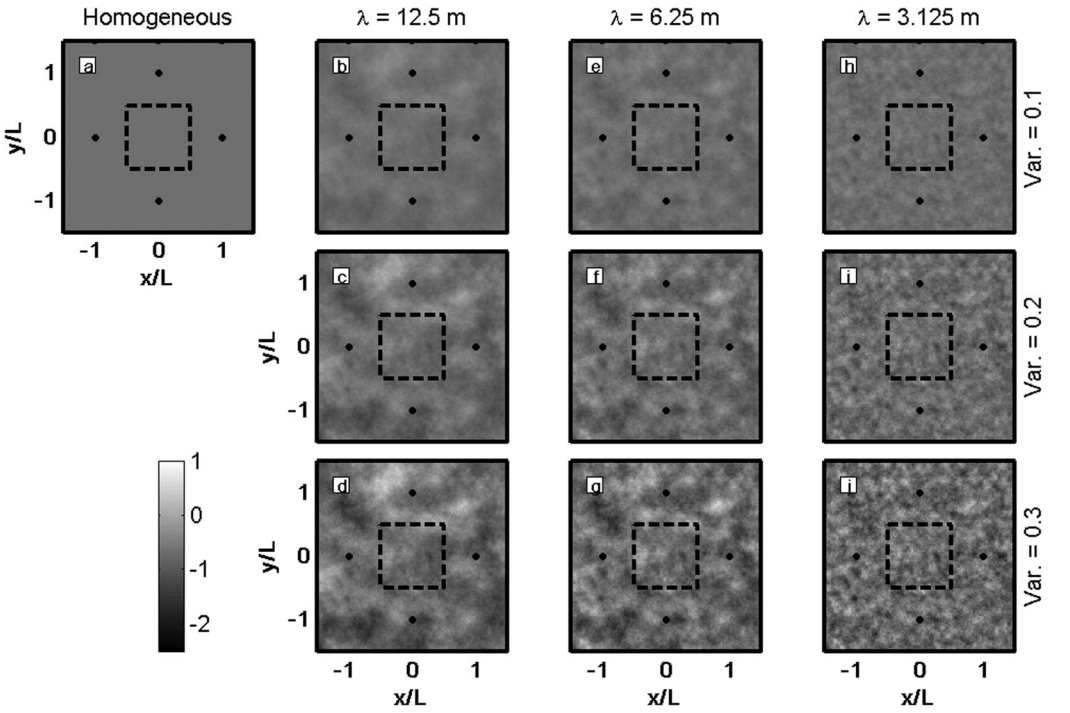

Figure 3. ln *T* fields (*T* in m^2/d) for the homogeneous aquifer and for one realization of a heterogeneous aquifer for each heterogeneity model. The black circles represent well locations. The dashed box represents the plot region in Figures 5 and 6.

The plume geometry after step 12 is shown in Figure 4 for the homogeneous aquifer and for the nine heterogeneous aquifers in Figure 3. For the heterogeneous aquifers, the interface is more irregular than the interface for the homogeneous aquifer. The deviation from the smooth three-branched shape increases as the variance of the random field increases (moving down a column in Figure 4) and as the correlation length decreases (moving across a row in Figure 4). This increased irregularity is caused by the increased velocity variations as the degree of heterogeneity increases.

For each heterogeneity model, we calculated the average (over all 30 realizations) interface length, ℓ_f, at the end of step 12 of the EIE sequence and the ratio of the final interface length to the initial interface length, $\ell_o = 39.3$m. The results, shown in column 3 of Table 3, show that the amount of stretching increases as the degree of heterogeneity increases (i.e., as $\sigma^2_{\ln T}$ increases for a given correlation length, or as λ decreases for a given variance of ln *T*).

3.2. Periodic Orbits

For the EIE sequence in Table 1, we identified period one points and their associated manifolds and orbits for the homogeneous aquifer and for the heterogeneous aquifers. Although periodic points of higher periods exist in this system, we did not identify them in this work for two reasons. First, period one points are expected to have the greatest impact on stretching [*Cvitanovic*, 1995]. Also, if treatment solution reaches an extraction well, the resulting degradation reactions can produce precipitates that can clog the well. For some of the heterogeneous aquifers used in this study, some treatment solution reaches an extraction well during the first or later cycle through the EIE sequence; thus, degradation reactions can occur in the well. To reduce the number of scenarios for which clogging may occur at the well, we simulate only one cycle of the EIE sequence, and therefore we identify only period one orbits.

3.2.1. Period One Points

To identify the period one points, we first identified regions that are nearly recurrent by creating a fine grid of numerical particles and tracking their advective movement through one cycle of the EIE sequence using MODFLOW and MODPATH. We calculated the separation distance between the original and final positions of each particle, and identified the locations for which the separation distance was small. Then, we refined

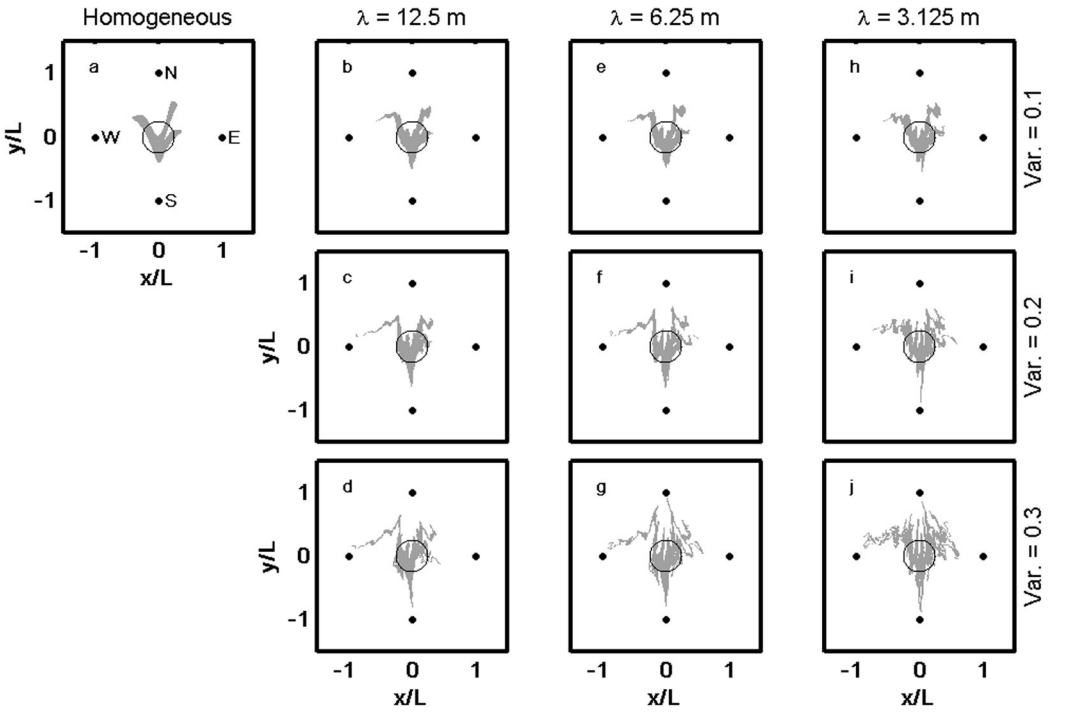

Figure 4. Position of the treatment solution plume (gray) at the end of the EIE sequence in the homogeneous aquifer and in one realization of a heterogeneous aquifer for each heterogeneity model. The open black circle shows the initial position of the treatment solution plume. Small filled black circles show the well locations.

the grid and repeated the process until we found locations for which the separation distance was near zero (less than $0.000011L$). Although this approach will find the majority of the periodic points, some periodic points may not have been found. Since we are interested in locations with significant stretching of the fluid interface, we limited our search to regions near the initial position of the treatment solution plume ($-0.5L \leq x \leq 0.5L; -0.5L \leq y \leq 0.5L$).

Figure 5 shows plots of the separation distances after one EIE cycle and the corresponding periodic points for the homogeneous aquifer and for the heterogeneous aquifers in Figure 3. For the homogeneous aquifer (Figure 5a), the separation distance plot shows four oval-shaped lobes within which the separation distance varies smoothly. The location of each periodic point, i.e., where the separation distance is near zero, occurs near the center of each lobe. The locations of these periodic points are very similar to the locations identified by *Mays and Neupauer* [2012] using an analytical flow model.

Table 3. Average Values of Stretching and Reaction Measures for Each Aquifer Model[a]

Aquifer Model									
λ (m)	$\sigma^2_{\ln T}$	ℓ_f/ℓ_o	Number of Period One Points	Manifold Stretch	Mass Degraded (%)	Average Filament Width (m)	Steady Flow ℓ_f/ℓ_o	Spatial Average Stretch	Probability of Extracting Treatment Solution
Homogeneous		2.4	4	4.7	62.4 (0.1)	3.07	1.5	0.45	0.10
12.5	0.1	4.9 (0.1)	4.5 (0.4)	11.5 (0.5)	62.6 (0.1)	1.95 (0.13)	1.69 (0.01)	0.93 (0.01)	0.52
12.5	0.2	13.6 (0.7)	9.3 (1.6)	25.0 (1.0)	63.0 (0.1)	0.628 (0.033)	2.03 (0.03)	1.61 (0.02)	0.68
12.5	0.3	30.5 (1.7)	13.5 (2.7)	41.5 (1.6)	63.8 (0.5)	0.278 (0.019)	2.47 (0.04)	2.25 (0.03)	0.78
6.25	0.1	7.3 (0.1)	7.7 (1.2)	14.5 (0.5)	63.0 (0.1)	1.15 (0.045)	1.80 (0.01)	1.26 (0.01)	0.57
6.25	0.2	25.7 (1.1)	13.0 (1.8)	45.4 (1.6)	64.2 (0.1)	0.314 (0.017)	2.34 (0.03)	2.29 (0.01)	0.71
6.25	0.3	69.1 (2.7)	15.0 (1.9)	90.9 (3.3)	66.1 (0.2)	0.118 (0.007)	3.05 (0.05)	3.22 (0.02)	0.84
3.125	0.1	11.7 (0.2)	9.2 (1.1)	23.4 (0.7)	63.2 (0.1)	0.658 (0.023)	1.97 (0.01)	1.74 (0.01)	0.43
3.125	0.2	52.6 (1.1)	10.5 (1.1)	91.4 (2.5)	65.1 (0.1)	0.143 (0.050)	2.80 (0.02)	3.14 (0.01)	0.78
3.125	0.3	188.7 (4.3)	11.7 (1.3)	249.2 (6.9)	67.7 (0.1)	0.0462 (0.0019)	3.83 (0.03)	4.38 (0.02)	0.90

[a]Standard errors in parentheses.

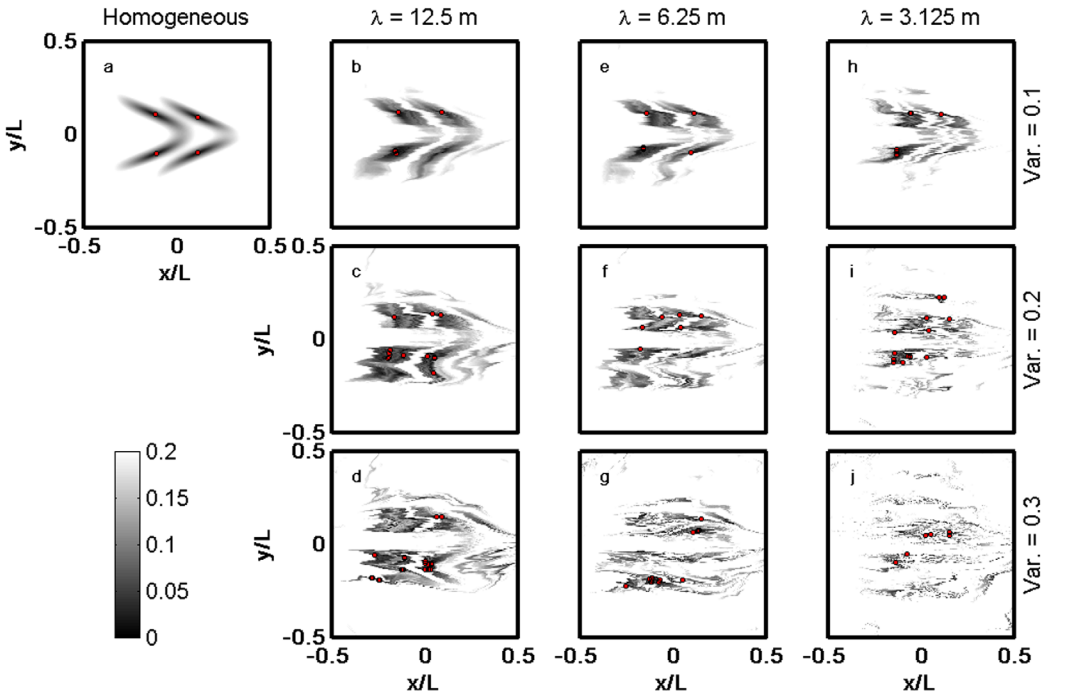

Figure 5. Dimensionless distance between initial and final particle positions after one cycle of the EIE sequence in the homogeneous aquifer and in one realization of a heterogeneous aquifer for each heterogeneity model. Red circles denote period one points.

As heterogeneity increases, the lobes of small separation distance fragment into complex structures, and the separation distance is no longer a smooth function of the initial position. The pattern of alternating high and low transmissivities causes some fluid to travel slightly faster than fluid adjacent to it, leading to more irregular structures of low separation distance as compared to the homogeneous aquifer case. The irregular structures have more local minima, although not all local minima are periodic points (i.e., the minimum separation distance may be greater than zero). Since our simulations use numerical methods, we may not have found all period one points, particularly where the bands of low separation distance are narrow compared to the finite difference grid spacing.

To characterize whether the periodic points were hyperbolic or elliptic, we tracked the movement of 10,000 numerical particles arranged in a circle of radius 0.01 L around each periodic point. Around an elliptic periodic point, where spreading is poor, the circle of particles would remain nearby although there would be shearing due to varying flow velocities with distance from the periodic point. Around a hyperbolic periodic point, where spreading is good, the circle of particles would be stretched along the unstable manifold. The slope of a line connecting the particles in the vicinity of the periodic point approximates the direction of the unstable manifold of the associated periodic point. We found that all of the periodic points were hyperbolic.

For each heterogeneity model, we calculated the average number (over all 30 realizations) of period one points for this EIE sequence. The results, shown in column 4 of Table 3, show that the number of period one points increases as $\sigma^2_{\ln T}$ increases. Since all period 1 points in this system are hyperbolic points that characterize good stretching, an increase in the number of period 1 points implies an increase in the amount of stretching. There is, however, no definite trend as the correlation length decreases. We believe this is due to the difficulty of identifying period one points when the separation distance plots have fine structure on the scale of the finite different grid. It is likely that some periodic points were not identified, particularly for the more heterogeneous aquifers.

3.2.2. Unstable and Stable Manifolds

The unstable and stable manifolds of the hyperbolic points characterize the stretching associated with the hyperbolic point. The manifolds generically have infinite length, so here we identify only segments of the manifolds in the vicinity of the periodic points. To identify the segment of the unstable manifold, we created

a line segment of length 0.025 L, represented by 10,000 numerical particles, centered at the periodic point and aligned in the direction of the unstable manifold, as determined by the slope of the line connecting the particles that was used to determine whether the periodic point was elliptic or hyperbolic. We tracked these particles through one cycle of the EIE system to obtain an unstable manifold segment (red lines in Figure 6). The segments of the stable manifolds (blue lines in Figure 6) were obtained in a similar process, tracking a small circle of particles through the EIE cycle in reversed time to find the slope of the stable manifold, and then tracking line segment of that slope centered at the periodic point through reversed time.

As the degree of heterogeneity increases, the manifold segments fill a larger portion of the domain. For example, for the homogeneous aquifer (Figure 6a), the manifold segments are very short, especially for the periodic points in the second and fourth quadrants. The space filled by the manifold segments increases as the variance of the random field increases (moving down a column in Figure 6) and as the correlation length decreases (moving across a row in Figure 6).

The degree of stretching around a periodic point can be quantified by the local eigenvalues of the Jacobian of the function that maps the periodic point back to itself after one EIE cycle [*Meiss*, 2007]. In this work, because flow is simulated numerically, we did not explicitly quantify the mapping function or the eigenvalues of its Jacobian. Instead, we quantified the degree of stretching by using a length stretch [*Ottino*, 1990], which is defined as the ratio of the final length of a curve after one cycle of the EIE system to the initial length. Here our curve is a segment of the unstable manifold, so we call this ratio the manifold stretch. The initial segment s_o is a vector of length 2 w (typically $w=0.01L$) attached to a period one points (x_p, y_p) in the direction of the unstable manifold. We put 1001 points along this vector, $s_o(k)=(x_p, y_p)+(k/N)w(\cos\theta, \sin\theta)$, where $k \in [-500, 500]$ and θ represents the angle of the manifold at the period one points. We then tracked each point through the EIE cycle to get $s_f(k)$. The total length of the final curve is then estimated as the sum of the lengths of the increments along the curve, using:

$$|s_f| = \sum_{k=-500}^{499} |s_f(k+1) - s_f(k)|. \tag{9}$$

The manifold stretch at a particular period one points is defined as $|s_f|/|s_o| = |s_f|/(2w)$.

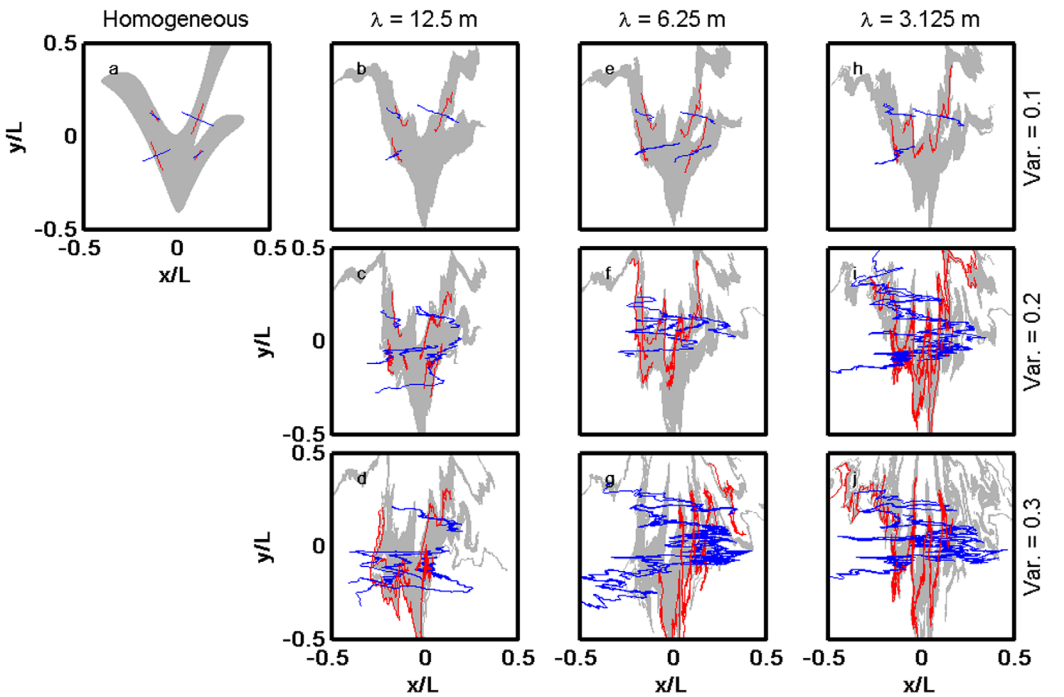

Figure 6. Treatment solution plume (gray) and segments of unstable (red) and stable (blue) manifolds after one cycle of the EIE sequence in the homogeneous aquifer and in one realization of a heterogeneous aquifer for each heterogeneity model.

For each heterogeneity model, we calculated the average (over all periodic orbits in all 30 realizations) manifold stretch for this EIE sequence. The results, shown in column 5 of Table 3, show that the average manifold stretch increases as the degree of heterogeneity increases (i.e., as $\sigma^2_{\ln T}$ increases for a given correlation length, or as λ decreases for a given variance of ln T). Heterogeneity leads to strong variations in the structure and stability properties of the periodic orbits, therefore some periodic orbits may exhibit substantially more stretching than others within the same realization or across realizations of the same heterogeneity model.

3.3. Contaminant Degradation

Since EIE is a method for remediating contaminated groundwater, the ultimate goal is the degradation of the contaminant. For each of the 30 realizations of each heterogeneity model, we solved (3) for both the contaminant and treatment solution concentrations using random walk with reaction using parameter values shown in Table 2. The initial plumes of treatment solution and contaminant (Figure 1) were represented by numerical particles initially placed on a regular grid with spacing of 0.01 L. The dispersion process for each particle was simulated with random displacements of mean zero and variance of $2\alpha_L|\mathbf{v}|\Delta t$ in the direction of the local velocity vector and $2\alpha_T|\mathbf{v}|\Delta t$ in the direction perpendicular to the local velocity vector, where Δt is the simulation time step. To obtain representative results, we ran 20 transport simulations for each transmissivity field realization. The average contaminant mass degraded during EIE is shown in column 6 of Table 3. The results show that as the degree of heterogeneity increases, the percentage of contaminant mass that is degraded during EIE also increases, although the relative increase is small compared to the increase in the manifold stretch.

3.4. Relationship Between Fluid Interface, Periodic Orbits, and Degradation

In a chaotic flow, stretching occurs not only near the periodic point, but also all along the entire unstable manifold; thus fluid that approaches a periodic orbit will, upon subsequent cycles, approach the path of the unstable manifold. In the context of groundwater remediation in the EIE system, wherever the interface falls near an unstable manifold, the interface will approach the unstable manifold at the end of each EIE sequence. Figure 6 shows that the fluid interface at the end of the EIE sequence aligns with the unstable manifolds of the period one points. As the degree of heterogeneity increases, the stretching of both the unstable manifolds and the interfaces also increases. Thus, a larger portion of the treatment solution has the opportunity to mix (through molecular diffusion and pore-scale dispersion) with the contaminated groundwater, which leads to more contaminant degradation during EIE in heterogeneous aquifers than in homogeneous aquifers. These results explain why the amount of contaminant mass that is degraded during EIE increases as the degree of heterogeneity increases.

Although the results (Table 3) show correlation between the length of the fluid interface and the percentage of contaminant mass that is degraded, the fluid interface increases by 2 orders of magnitude from the homogeneous aquifer to the most heterogeneous aquifer, while the percentage of mass that is degraded increases by only a few percent. The fine-scale plume structure, such as that shown in Figure 4j, leads to a very large interface length. As the interface length increases, the plume shape is characterized by narrow filaments. If the filament width is small compared to the dispersion length scale, dispersion smooths out the filaments and the effective interface length, across which molecular diffusion will bring contaminant and treatment solution particles together, is much smaller than the actual interface length that results from advective transport only.

We define the dispersion length scale λ_D as:

$$\lambda_D = \sqrt{2\alpha_T|\mathbf{v}|\Delta t}, \tag{10}$$

where $|\mathbf{v}|$ is the magnitude of the groundwater velocity vector and t is a time scale. We use the duration of an EIE step ($t = 6.25$ days) as the time scale. Since velocity varies spatially and temporally, the dispersion length scale also varies in space and time. To obtain a typical dispersion length scale, we calculated the dispersion length scale at the origin during each step of the EIE sequence for a homogeneous aquifer. These dispersion length scales range from $\lambda_D = 0.10$ m for EIE steps 3 and 9, to $\lambda_D = 0.18$ m for EIE steps 1, 2, 7, and 8.

We calculated the average filament width for the final configuration of the treatment solution plume for each realization; these values are reported in column 7 of Table 3. The average filament with was calculated as the

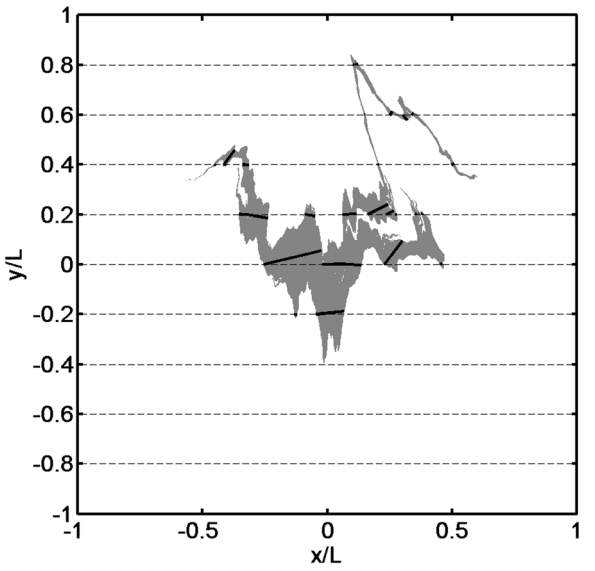

Figure 7. Final configuration of the treatment solution plume (gray) for one realization of the heterogeneity model for λ=6.25 m and $\sigma^2_{\ln T}$=0.2. The thick black lines show the locations where the plume widths were measured, which coincides with the locations where the plume interface crosses the transects shown by the dashed lines.

average of the width of the plume perpendicular to the interface at all points where the interface crossed transects at $y=0L, \pm 0.2L, \pm 0.4L, \ldots$, as shown in Figure 7. For most of the aquifer heterogeneity models, the filament width is on the same order of magnitude as the dispersion length scale. These results demonstrate that while spreading due to chaotic advection and heterogeneity leads to a long fluid interface which allows more opportunity for diffusive mixing to bring together the treatment solution and contaminant to react, the transverse dispersion process may play a more dominant role in reaction for the more heterogeneous aquifers.

4. Discussion

EIE creates a time-dependent flow field that leads to stretching and folding of the treatment solution and contaminant plumes, and ultimately to more contaminant degradation. In this section, we discuss the relationship between the observed features of chaotic advection and the effects of the EIE system on the contaminated aquifer.

4.1. Comparison With Transport and Reaction in a Steady Flow Field

To evaluate the effectiveness of EIE, we simulated the movement of the treatment solution plume in a steady flow field, in which water is injected into the west well at a rate of 583 m^3/d, equivalent to the average of the magnitudes of the injection rates of the EIE sequence. We simulate the movement of the treatment solution plume over a 75 day period, which is equivalent to the duration of the EIE sequence in Table 1 and results in the same volume of water injected as with EIE. The final position and geometry of the treatment solution plume is shown in Figure 8 for the homogeneous aquifer and for one realization of each heterogeneous aquifers. We calculated the average final interface length, ℓ_f, for each heterogeneity model (over all 30 realizations) and reported the degree of stretching of the interface, quantified as ℓ_f/ℓ_o, in column 8 of Table 3. The results show that even with steady flow, the spatial velocity variations in heterogeneous aquifers lead to more stretching of the interface as compared to the homogeneous aquifer. The final interface length in the most heterogeneous aquifer is 2.5 times larger than that in the homogeneous aquifer. Although aquifer heterogeneity leads to stretching of the interface in steady flow, more stretching is produced by EIE than by steady flow alone for all aquifers. For example, for the heterogeneous aquifer with λ= 6.25 m and $\sigma^2_{\ln T}$=0.2, the length of the interface after EIE is over 10 times longer than the length of the interface in steady flow in the same aquifer; thus EIE leads to a 10-fold increase in the interface length (when neglecting dispersion). On the other hand, the length of the interface in steady flow in this heterogeneous aquifer is increased by only 50% as compared to the length of the interface in steady flow in the homogeneous aquifer; thus, heterogeneity leads to a 50% increase in the interface length, which is much less than the increase due to EIE alone. Note also that the combined effects of EIE and heterogeneity produce substantially more stretching than EIE alone and than heterogeneity alone.

4.2. Spatial Average Stretching

We illustrate the degree of stretching throughout the domain using the spatial distribution of a local length stretch and a spatial average stretch, which has been studied as a measure of chaos in many dynamical systems [*Franjione and Ottino*, 1987; *Ottino*, 1989; *Boyland et al*., 2003]. In the infinite-time limit, the spatial average stretch gives an estimate of the so-called topological entropy [*Thiffeault*, 2004]. Formally, the entropy measures the information lost per unit time when measurements are made at finite precision. It can also be

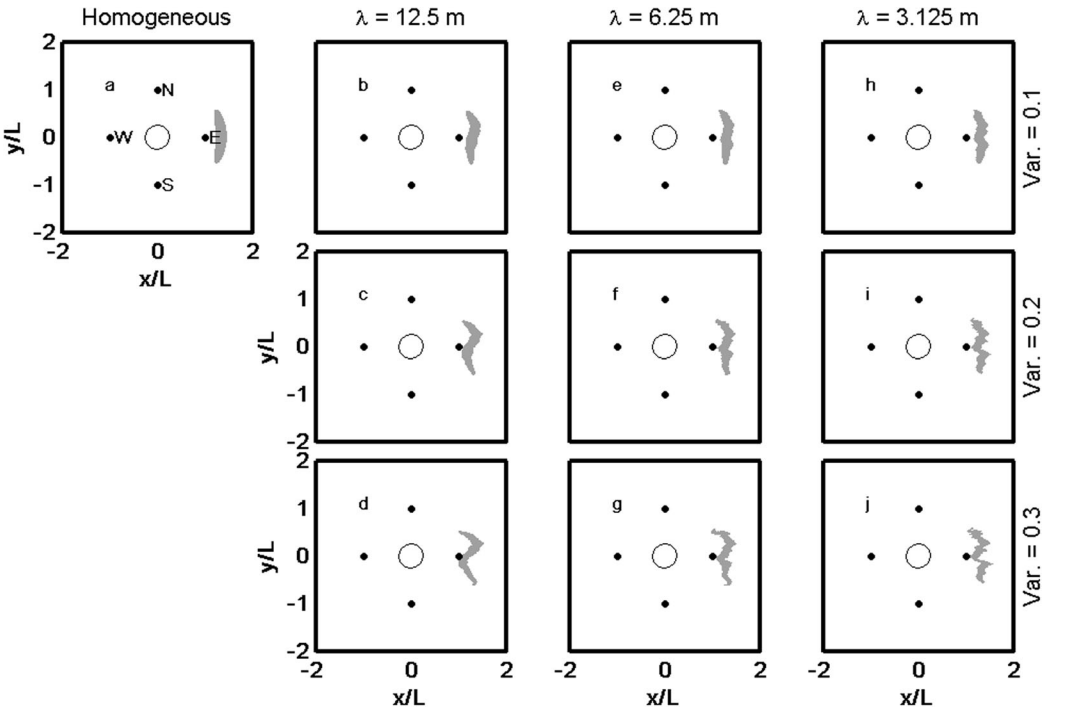

Figure 8. Treatment solution plume (gray) after 75 days of transport in a steady flow field in the homogeneous aquifer and in one realization of a heterogeneous aquifer for each heterogeneity model. The open black circle represents the initial position of the treatment solution plume. The filled black circles represent the well locations.

defined as the growth rate of the number of distinguishable orbits on a given measurement scale. The topological entropy is a fundamental measure of chaos: a dynamical system is chaotic whenever there is an invariant set that has positive topological entropy.

We calculate the local length scale on a regular grid ranging from x_o to $x_o+N_x\Delta x$ in the x direction and from y_o to $y_o+N_y\Delta y$ in the y direction. Let $c_o(x_i, y_j)$ denote a circle that satisfies the equation:

$$(x-x_i)^2+(y-y_j)^2=r^2, \tag{11}$$

where $x_i=x_o+i\Delta x, y_j=y_o+j\Delta y$ and r is the radius of the circle. Let $c_f(x_i, y_j)$ be the curve obtained by tracking $c_o(x_i, y_j)$ through the 12 steps of the EIE cycle. We define the local length stretch, $\gamma(x_i, y_j)$, as the ratio of the length of the curve represented by $c_f(x_i, y_j)$ to the circumference of $c_o(x_i, y_j)$. We represented $c_o(x_i, y_j)$ with 1000 uniformly spaced numerical particles, with $r=0.01L$. We used $(x_o, y_o)=(-0.25L, -0.25L)$, $\Delta x=\Delta y=0.025L$, and $N_x=N_y=21$. The spatial average stretch, Γ, is defined as the spatial average of the natural logarithm of the local length stretch, given by:

$$\Gamma=\frac{1}{N_xN_y}\sum_{i=0}^{N_x-1}\sum_{j=0}^{N_y-1}\ln\left[\gamma(x_i, y_j)\right]. \tag{12}$$

The natural logarithm of the local length stretch is shown in Figure 9, and the spatial average stretch is reported in column 9 of Table 3. These results show that stretching occurs throughout the plot domain, and that the local and spatial average stretches increase as the degree of heterogeneity increases. Within each aquifer, the most substantial stretching occurs near the stable manifolds (compare Figures 6 and 9). To explain this behavior, Figure 10 shows the unstable and stable manifolds for the period one point in the first quadrant in the homogeneous aquifer. Two fluid particles, labeled "1" and "2" are initially near each other, but on opposite sides of the stable manifold. The thick black lines show a schematic of the path of these fluid particles in subsequent cycles of the EIE sequence. The particles initially move toward the periodic

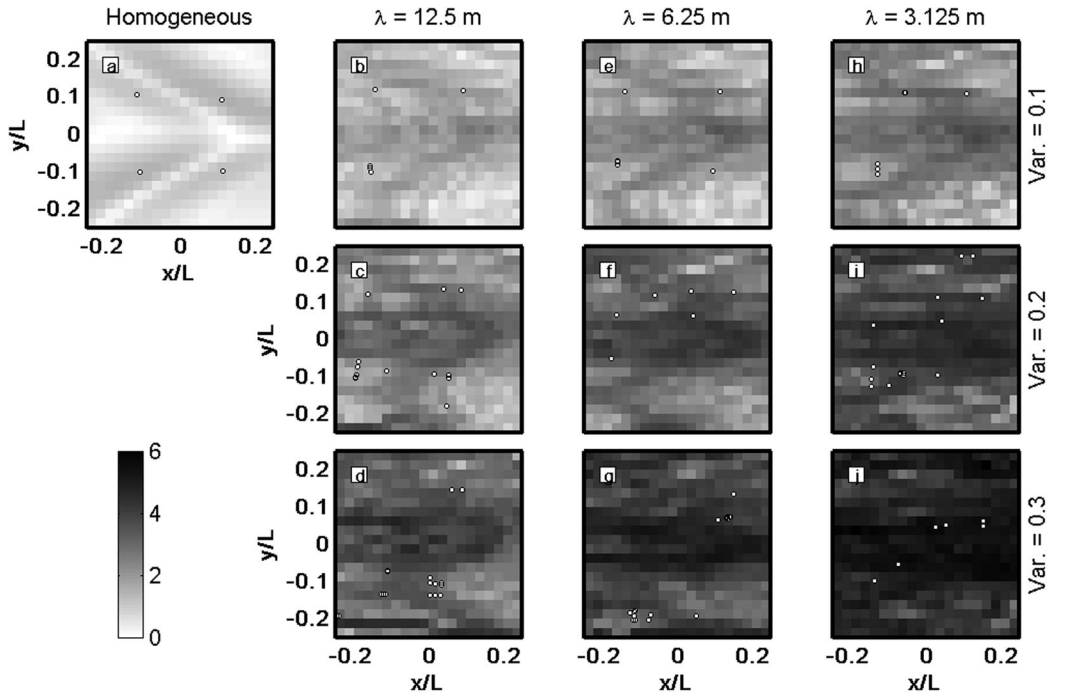

Figure 9. Spatial distribution of natural logarithm of the local length stretch during one cycle of the EIE sequence in the homogeneous aquifer and in one realization of a heterogeneous aquifer for each heterogeneity model. White circles represent period one points.

point, and eventually approach the unstable manifold. Since their original positions were on opposite sides of the stable manifold, they move in opposite directions along the unstable manifold, leading to significant stretching.

4.3. Implications

The hydraulic conductivity fields evaluated in this study have a mild degree of heterogeneity, with $\sigma^2_{\ln T} \leq 0.3$. We have shown that even this mild degree of heterogeneity significantly enhances plume spreading during EIE. Presumably, if EIE were conducted in aquifers with moderate or high degrees of heterogeneity, even more stretching of the interface would occur, potentially leading to more opportunities for degradation reactions. However, with more stretching, the interface, and therefore the treatment solution, is more likely to reach an extraction well during EIE, increasing the risk of clogging and raising regulatory concerns [*Mays and Neupauer*, 2013]. Table 3 (column 10) shows the probability that any treatment solution reaches an extraction well during a reactive transport simulation (20 simulations of each of the 30 realizations, for a total of 600 simulations for each heterogeneity model). In general, the probability increases as the degree of heterogeneity increases. As such, conducting EIE in heterogeneous aquifers can have competing benefits (enhanced reaction) and drawbacks (clogging, regulatory issues).

To avoid extracting treatment solution at the wells, the wells can be moved farther away or the injection and extraction rates can be reduced. In doing so, however, the degree of stretching and the amount of contaminant degradation will be reduced. We demonstrate here how reducing the injection and extraction impacts stretching and degradation. We consider the homogeneous aquifer and one realization of the heterogeneity model for λ=6.25m and $\sigma^2_{\ln T}$=0.2. We scaled the injection and extraction rates by a factor of $\beta < 1$. For the homogeneous aquifer, scaling all injection and extraction rates by a factor of β is equivalent to moving the wells to a distance of $\beta^{-1/2}L$ from the origin [*Mays and Neupauer*, 2012]. The results are shown in Table 4.

For both aquifers, β can be reduced to a level where the probability of extracting treatment solution is zero (based on 20 reactive transport simulations). To achieve this level, a lower β is required for the heterogeneous aquifer because connected high-transmissivity paths allow the treatment solution to travel farther

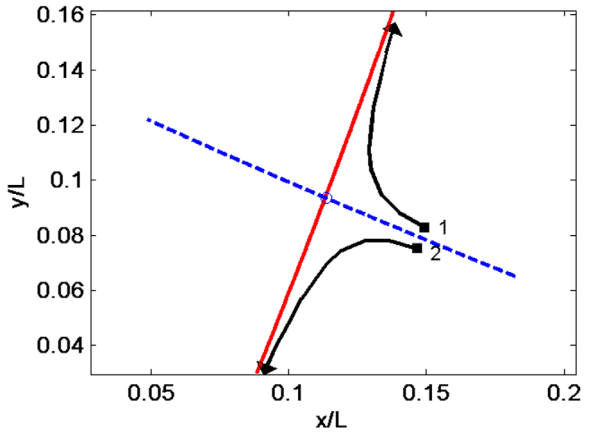

Figure 10. Unstable (red line) and stable (blue dashed line) manifolds of a period one point (circle) in the homogeneous aquifer. Black squares represent initial positions of two fluid particles. The thick black lines represent schematics of the fluid particle paths through subsequent cycles of the EIE sequence, with the arrows indicating the direction of movement.

distances in the heterogeneous aquifer than in the homogeneous aquifer for the same injection or extraction rates. The results show that as β decreases, all measures of stretching decrease, and the amount of contaminant degradation decreases. The one exception is in the number of period one points, which increases for $\beta = 0.8$ in the heterogeneous aquifer. The locations of the periodic points change when the flow conditions change, and thus the number of periodic points can change because the flow near the periodic points samples different heterogeneity structures.

The decrease in contaminant degradation is on the order of 1–2% for a 10% decrease in β, while the decrease in the probability of extracting treatment solution is more substantial. A full optimization of the EIE sequence would be necessary to balance the trade-offs between reducing the probability of extracting treatment solution and maximizing the amount of degradation. This optimization is beyond the scope of this paper, and is the topic of ongoing research.

5. Conclusions

We investigated the effects of aquifer heterogeneity on chaotic advection created by engineered injection and extraction. We simulated EIE in a homogeneous aquifer and in heterogeneous aquifers, and we analyzed the chaotic features of the resulting flows.

Hyperbolic periodic points represent areas of good spreading. A fluid parcel at a hyperbolic periodic point is stretched in the direction of the unstable manifold and is compressed in the direction of the stable manifold. We found that as the degree of heterogeneity increases, the degree of stretching along the unstable manifold also increases.

We have shown that the interface between the treatment solution and contaminated groundwater at the end of the EIE sequence is aligned closely with the unstable manifolds of the hyperbolic periodic points. Thus, the fluid interface experiences more stretching in flows in heterogeneous aquifers, for which the manifolds exhibit high degrees of stretching. The additional stretching of the fluid interface allows more treatment solution to come into contact with contaminated groundwater, leading to more opportunities for degradation reactions to occur.

Engineered injection and extraction spreads a treatment solution into the contaminated groundwater, increasing the amount of contact between the treatment solution and contaminant, thereby increasing the

Table 4. Stretching and Reaction Measures for Reduced Injection and Extraction Rates

	Homogeneous		Heterogeneous		
Parameter	$\beta = 1$	$\beta = 0.9$	$\beta = 1$	$\beta = 0.9$	$\beta = 0.8$
ℓ_f/ℓ_o	2.4	1.7	31.6	17.9	11.6
Number of period one points	4	4	8	4	28
Manifold stretch	4.7	2.1	46.4	44.3	37.8
Mass degraded (%)	62.4	60.9	61.7	61.4	59.5
Filament width (m)	3.1	5.8	0.24	0.43	0.85
Global length stretch	0.45	0.40	2.34	2.24	2.02
Probability of extracting treatment solution	0.10	0.00	1.00	0.40	0.00

rate and spatial extent of degradation reactions that occur. In a homogeneous aquifer, all of the spreading is caused by the spatially varying velocity created by the EIE system. In a heterogeneous aquifer, additional spreading occurs as a result of the spatial variability in aquifer properties, causing the EIE system to be even more effective in remediating a contaminated aquifer. We have shown that the amount of contaminant mass that is degraded during EIE increases as the degree of heterogeneity increases, although the rate of increase is much lower than the rate of increase in the stretching. Dispersion blurs the fluid interface, and eliminates the fine structure of the treatment solution plume, leading to a reaction zone that is shorter than the simulated interface length. Nevertheless, increased aquifer heterogeneity leads to increased plume spreading and increased contaminant degradation in the EIE system.

Acknowledgments
This work was funded by the National Science Foundation under grants DMS-1211350, EAR-1113996, and EAR-1114060. The authors thank Mathew Accardo for performing numerical simulations used in this work. Three reviewers, the associate editor, and the editor provided useful comments that improved this manuscript.

References

Bagtzoglou, A. C., and P. M. Oates (2007), Chaotic advection and enhanced groundwater remediation, *J. Mater. Civ. Eng.*, *19*(1), 75–83.
Boyland, P. L., M. A. Stremler, and H. Aref (2003), Topological fluid mechanics of point vortex motions, *Physica D*, *175*, 69–95.
Cirpka, O. A., R. L. Schwede, J. Luo, and M. Dentz (2008), Concentration statistics for mixing-controlled reactive transport in random heterogeneous media, *J. Contam. Hydrol.*, *98*, 61–74.
Cirpka, O. A., F. P. J. de Barros, G. Chiogna, M. Rolle, and W. Nowak (2011), Stochastic flux-related analysis of transverse mixing in two-dimensional heterogeneous porous media, *Water Resour. Res.*, *47*, W06515, doi:10.1029/2010WR10279.
Cvitanovic, P. (1995), Dynamical averaging in terms of periodic orbits, *Physica D*, *83*(1–3), 109–123.
Dagan, G. (1984), Solute transport in heterogeneous formations, *J. Fluid Mech.*, *145*, 151–177.
Dagan, G. (1989), *Flow and Transport in Porous Formations*, Springer, New York.
De Simoni, M., J. Carrera, X. Sanchez-Vila, and A. Guadagnini (2005), A procedure for the solution of multicomponent reactive transport problems, *Water Resour. Res.*, *41*, W11410, doi:10.1029/2005WR004056.
Dentz, M., T. Le Borgne, A. Englert, and B. Bijeljic (2011), Mixing, spreading and reaction in heterogeneous media: A brief review, *J. Contam. Hydrol.*, *120–121*, 1–17, doi:10.1016/j.conhyd.2010.05.002.
Deutsch, C., and A. Journel (1992), *GSLIB: Geostatistical Software Library and User's Guide*, Oxford Univ. Press, New York.
Franjione, J. G., and J. M. Ottino (1987), Feasibility of numerical tracking of material lines and surfaces in chaotic flows, *Phys. Fluids*, *30*(12), 3641–3643.
Gelhar, L. W., and C. L. Axness (1983), Three-dimensional stochastic analysis of macrodispersion in aquifers, *Water Resour. Res.*, *19*(1), 161–180.
Harbaugh, A. W., E. R. Banta, M. C. Hill, and M. G. McDonald (2000), MODFLOW-2000, The U.S. Geological Survey modular ground-water model—User's guide to modularization concepts and the ground-water flow process, *Open File Rep. 00–92*, U.S. Geol. Surv., Reston, Va.
Jones, S. W. and H. Aref (1988), Chaotic advection in pulsed source sink systems, *Phys. Fluids*, *31*(3), 469–485.
Le Borgne, T., M. Dentz, D. Bolster, J. Carrera, J. R. de Dreuzy, and P. Davy (2010), Non-Fickian mixing: Temporal evolution of the scalar dissipation rate in heterogeneous porous media, *Adv. Water Resour.*, *33*(12), 1468–1475.
Luo, J., M. Dentz, J. Carrera, and P. Kitanidis (2008), Effective reaction parameters for mixing controlled reactions in heterogeneous media, *Water Resour. Res.*, *44*, W02416, doi:10.1029/2006WR005658.
Mays, D. C., and R. M. Neupauer (2012), Plume spreading in groundwater by stretching and folding, *Water Resour. Res.*, *48*, W07501, doi:10.1029/2011WR011567.
Mays, D. C., and R. M. Neupauer (2013), Reply to comment by D.R. Lester et al. on "Plume spreading in groundwater by stretching and folding", *Water Resour. Res.*, *49*, 1192–1194, doi:10.1002/wrcr.20081.
Meiss, J. D. (2007), *Differential Dynamical Systems*, Soc. for Ind. and Appl. Math., Philadelphia, Pa.
Mosovsky, B. A., and J. D. Meiss (2011), Transport in transitory dynamical systems, *SIAM J. Dyn. Syst.*, *10*(1), 35–65.
Ottino, J. M. (1989), *The Kinematics of Mixing: Stretching, Chaos, and Transport*, Cambridge Univ. Press, Cambridge, U. K.
Ottino, J. M. (1990), Mixing, chaotic advection, and turbulence, *Annu. Rev. Fluid Mech.*, *22*, 207–253.
Ottino, J. M., S. C. Jana, and V. S. Chakravarthy (1994), From Reynolds stretching and folding to mixing studies using horseshoe maps, *Phys. Fluids*, *6*(2), 685–699.
Piscopo, A. M., D. C. Mays, and R. M. Neupauer (2013), Engineered injection and extraction to enhance reaction for improved in situ remediation, *Water Resour. Res.*, *49*, 3618–3625, doi:10.1002/wrcr.20209.
Pollock, D. W. (1994), User's guide for MODPATH/MODPATH-PLOT, Version 3: A particle tracking post-processing package for MODFLOW, The U.S. Geological Survey finite-difference ground-water flow model, *Open File Rep. 94–464, U.S. Geol. Surv.*, Reston, Va.
Schafer-Perini, A., and J. L. Wilson (1991), Efficient and accurate front tracking for two-dimensional groundwater-flow models, *Water Resour. Res.*, *27*(7), 1471–1485.
Sposito, G. (2006), Chaotic solute advection by unsteady groundwater flow, *Water Resour. Res.*, *42*, W06D03, doi:10.1029/2005WR004518.
Stremler, M. A., F. R. Haselton, and H. Aref (2004), Designing for chaos: Applications of chaotic advection at the microscale, *Philos. Trans. R. Soc. London A*, *362*(1818), 1019–1036.
Tabor, M. (1989), *Chaos and Integrability in Nonlinear Dynamics*, John Wiley, New York.
Tel, T., G. Karolyi, A. Pentek, I. Scheuring, Z. Toroczkai, C. Grebogi, and J. Kadtke (2000), Chaotic advection, diffusion, and reactions in open flows, *Chaos*, *10*(1), 89–98.
Thiffeault, J. L. (2004), Stretching and curvature of material lines in chaotic flows, *Physica D*, *198*, 169–181.
Trefry, M., D. Lester, G. Metcalfe, A. Ord, and K. Regenauer-Lieb (2012), Toward enhanced subsurface intervention methods using chaotic advection, *J. Contam. Hydrol.*, *127*(1–4), 15–29.
Wiggins, S. (2010), Coherent structures and chaotic advection in three dimensions, *J. Fluid Mech.*, *654*, 1–4.